



## Multi-layer membrane model for mass transport in a direct ethanol fuel cell using an alkaline anion exchange membrane

Hafez Bahrami, Amir Faghri\*

Department of Mechanical Engineering, University of Connecticut, Storrs, CT 06269, USA

### HIGHLIGHTS

- The first physical model for AEM-DEFCs is presented.
- The necessity of employing multi-layer membrane model is outlined.
- Details of electroosmotic and diffusive ethanol crossover are discussed.
- Fuel crossover is significantly reduced in AEM-DEFCs.

### ARTICLE INFO

#### Article history:

Received 14 May 2012

Accepted 15 June 2012

Available online 8 July 2012

#### Keywords:

DEFC

Crossover

Alkaline anion exchange membrane

Ethanol

Fuel cell

### ABSTRACT

A one-dimensional, isothermal, single-phase model is presented to investigate the mass transport in a direct ethanol fuel cell incorporating an alkaline anion exchange membrane. The electrochemistry is analytically solved and the closed-form solution is provided for two limiting cases assuming Tafel expressions for both oxygen reduction and ethanol oxidation. A multi-layer membrane model is proposed to properly account for the diffusive and electroosmotic transport of ethanol through the membrane. The fundamental differences in fuel crossover for positive and negative electroosmotic drag coefficients are discussed. It is found that ethanol crossover is significantly reduced upon using an alkaline anion exchange membrane instead of a proton exchange membrane, especially at current densities higher than  $500 \text{ A m}^{-2}$ .

© 2012 Elsevier B.V. All rights reserved.

### 1. Introduction

An extensive, worldwide search for safe, renewable and sustainable sources of energy is underway. As an alternative to conventional power providers such as gas turbines and internal combustion engines operating on a thermal cycle, the fuel cell technology has been considered as a promising source of clean energy. Fuel cells directly convert the chemical energy of fuel to the electricity and are not limited by the maximum Carnot efficiency. Hydrogen is the most commonly used fuel in fuel cells, especially in a proton exchange membrane type. Issues regarding storing, handling, transporting and production of hydrogen led us to consider energy-dense and hydrogen-rich liquid alcohols such as methanol and ethanol.

Methanol is the most attractive alternative due to its large hydrogen to carbon ratio in the molecular structure. During the past decade, extensive research efforts have been focused on the

study of the direct methanol fuel cell (DMFC) [1,2]. In addition to the obstacle of methanol crossover [3,4] and the sluggish kinetics of methanol oxidation [5], the toxicity of methanol presents a major disadvantage. Ethanol, on the other hand, offers a higher specific energy ( $30 \text{ MJ kg}^{-1}$ ) than methanol ( $19.7 \text{ MJ kg}^{-1}$ ) and is safe and renewable. Ethanol is the mass produced by fermentation of sugar-containing biomass such as sugar cane, corn and wheat.

Early efforts to use ethanol were based on DMFC technology and using Nafion as a membrane in an acidic medium. It demonstrated a poor performance compared to methanol, nearly 1/7 of maximum power density of methanol at room temperature [6]. Recently, the novel idea of changing the reacting medium from an acid-base to alkali-base has made a breakthrough improvement in employing ethanol as a sustainable energy source [6]. The alkaline medium is provided by employing an anion exchange membrane (AEM). Utilizing an alkaline medium versus an acidic medium offers several benefits including: (i) improved oxygen reduction and ethanol oxidation which allows the use of non-noble catalysts, (ii) better corrosion resistance, and (iii) negative electro-osmotic drag, mitigated fuel crossover and resulting less potential water flooding in the cathode.

\* Corresponding author. Tel.: +1 860 486 0419.

E-mail addresses: [hafezbahrami@gmail.com](mailto:hafezbahrami@gmail.com) (H. Bahrami), [faghri@engr.uconn.edu](mailto:faghri@engr.uconn.edu) (A. Faghri).

## Nomenclature

	<i>Greek</i>
AEM	Anion Exchange Membrane
AEM-DEFC	Direct ethanol fuel cell using an AEM
C	Concentration, mol·m <sup>-3</sup>
CL	Catalyst layer
DEFC	Direct ethanol Fuel Cell
D	Diffusivity, m <sup>2</sup> ·s <sup>-1</sup>
DL	Diffusion layer
DMFC	Direct Methanol Fuel Cell
<i>E</i> <sub>rev</sub>	Reversible cell voltage, V
F	Faraday constant, 96,485.3, A s mol <sup>-1</sup>
G	Gibbs energy, J
H	Enthalpy, J
I	Current density, A m <sup>-2</sup>
<i>I</i> <sub>p</sub>	Parasitic current, A m <sup>-2</sup>
<i>J</i> <sub>0,O<sub>2</sub></sub> <sup>ref</sup>	Reduction exchange current density, A m <sup>-3</sup>
<i>J</i> <sub>O,e</sub> <sup>ref</sup>	Oxidation exchange current density, A m <sup>-3</sup>
L	Length, m
n	Number of computational node (layer)
<i>n</i> "	Molar flux, mol m <sup>-2</sup> s <sup>-1</sup>
<i>n</i> <sub>d</sub>	Electroosmotic coefficient
R	Reaction rate, A m <sup>-3</sup>
R <sub>u</sub>	Universal gas constant, 8.3145 J mol <sup>-1</sup> K <sup>-1</sup>
R <sub>con</sub>	Contact resistance, Ω m <sup>2</sup>
R <sub>r</sub>	Internal resistance, Ω m <sup>2</sup>
S	Entropy, J K <sup>-1</sup>
s	Liquid saturation
T	Temperature, K
u	Velocity, m s <sup>-1</sup>
U	Thermodynamic equilibrium potential, V
V	Voltage, V
x	Coordinate for mass transport in the cell, m, or mole fraction
x'	Coordinate for charge transport in the anode catalyst layer, m
x"	Coordinate for charge transport in the cathode catalyst layer, m
	<i>Greek</i>
	α Transfer coefficient
	γ Reaction order
	ε Porosity of porous medium
	η Overpotential, V
	ρ Density, kg m <sup>-3</sup>
	σ Conductivity, Ω <sup>-1</sup> m <sup>-1</sup>
	ϕ Phase potential, V
	<i>Superscripts</i>
	CL Catalyst
	eff effective
	ref Reference value
	<i>Subscripts</i>
	a Anode
	AEM Anion Exchange Membrane
	amb Ambient
	c Cathode
	car Carbon
	CL Catalyst
	cr Crossover
	d Drag
	D Diffusive
	e Ethanol or electron
	E Electroosmosis
	el-ch Electrochemical
	H <sub>2</sub> O Water
	KOH Potassium hydroxyl
	lim Limiting value
	mem Membrane phase
	o Standard condition of T = 298 K and P = 1 atm
	ox Oxidation
	O <sub>2</sub> Oxygen
	OH Hydroxyl ion
	p Parasitic
	red Reduction
	res Reservoir
	0 x' = 0 or x" = 0

During the past few years, there have been increasing research interests in various aspects of a direct ethanol fuel cell using an AEM, known as an AEM-DEFC. Table 1 presents a summary of the experimental studies conducted on the AEM-DEFC performance and design.

The table is broken down into active and passive AEM-DEFCs. In an active system, fuel and oxidant are forced through the channels, whereas in a passive system there are no moving parts. There are, in general, two types of AEMs: (i) AEMs with a quaternary ammonium functional group and (ii) polybenzimidazole (PBI) doped in strong bases. The former is usually known as the name of its major supplier, Tokuyama, and the latter benefits from the higher ion conductivity (up to 9 Ω<sup>-1</sup>m<sup>-1</sup>) [19]. Tokuyama membrane (denoted by T in the second column of Table 1), Pd-based catalyst for the anode and Fe–Co based catalysts for the cathode are most commonly used. Adding a hydroxyl source to the inlet fuel is necessary to increase the ion conductivity of the AEM and to improve the kinetics of ethanol oxidation reaction (EOR). Both KOH and NaOH may be added to the anode side. In all the studies conducted, it was preferable to use KOH rather than NaOH as the hydroxyl source in the anode channel, because KOH solution has a higher ionic conductivity than a NaOH solution under the same conditions. More importantly, both K<sub>2</sub>CO<sub>3</sub> and CH<sub>3</sub>COOK have

much higher solubility in the water than Na<sub>2</sub>CO<sub>3</sub> and CH<sub>3</sub>COONa [20]. The highest reported power density for an AEM-DEFC is 170 mW·cm<sup>-2</sup> at 80 °C using pure oxygen in the cathode for the active mode [11] and 65 mW·cm<sup>-2</sup> at 80 °C using air in the cathode for the passive mode [18].

To the authors' knowledge, there is no reported physical model for transport phenomena in an AEM-DEFC. From a practical perspective, thorough knowledge of mass transport, which is difficult to obtain through the experimental measurements, is of enormous importance for the further development of this type of fuel cell. The objective of this study is to provide detailed insight concerning the mass transport in an AEM-DEFC incorporating the negative electroosmotic drag. A multi-layer membrane model is proposed to investigate the fundamental influences of using an alkaline membrane in reducing ethanol crossover. The electrochemistry is analytically solved, and the closed-form solution is provided for two limiting cases. Ethanol crossover is substantially reduced when an AEM is used compared to the conventional proton exchange membrane.

## 2. Formulation

The general structure of an AEM-DEFC is very similar to a DMFC. It composes of a diffusion layer (DL) and a catalyst layer (CL) in both

**Table 1**

Summary of the experimental studies for AEM-DEFCs.

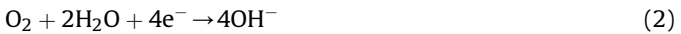
Investigator	AEM	KOH concentration, M	Anode catalyst	Cathode catalyst	Max $P$ (mW cm $^{-2}$ )	Temperature, °C	Anode fuel ethanol, M	Ethanol flow rate, ml min $^{-1}$	Cathode fuel	Oxidant flow rate, ml min $^{-1}$
<i>Active</i>										
Fujiwara et al. [6], 2008	T <sup>a</sup>	0.5	Pt/Ru	Pt black	58	25	1	4	O <sub>2</sub>	100
Hou et al. [7], 2008	P <sup>b</sup>	2	Pt/Ru/C	Pt/C	49.2	75	2	1	O <sub>2</sub>	–?
Modestov et al. [8], 2009	P	3	Ru–V/C	TMPPhP–Co/C	100	80	2	5	Air	200
Li et al. [9], 2009	T	1	Ni–Fe–Co K	Fe–CO K <sup>c</sup>	60	40	1	1	O <sub>2</sub>	10
Li et al. [10], 2009	T	7	Ni–Fe–Co K	Fe–CO K	60	40	3	2	O <sub>2</sub>	10
Bianchini et al. [11], 2009	T	2	Pd–(Ni–Zn)/C	Fe–CO K	170	80	10 W <sup>d</sup>	4	O <sub>2</sub>	200
Bambagioni et al. [12], 2009	T	2	Pd/MWCNT	Fe–CO K	73	80	10 W	4	O <sub>2</sub>	200
Shen et al. [13], 2010	T	1	Pd–Ni/C	Fe–CO K	44	60	1	1	O <sub>2</sub>	10
		5			90	60	3	1	O <sub>2</sub>	10
Li and Zhao [14], 2011	T	5	Pd–Ni/C	Fe–CO	130	80	3	1	O <sub>2</sub>	10
Zhiani et al. [15], 2011	T	10 W	K	K	87	60	10 W	7	Air	150
Mazin et al. [16], 2011	FF <sup>e</sup>	2	Ru–V/C	Co–TMPP	45	32	1	210	O <sub>2</sub>	5
Shen et al. [17], 2011	T	5	Pd–Ni–Ir/C	Fe–CO	60	90	3	1	O <sub>2</sub>	10
<i>Passive</i>										
Bianchini et al. [11], 2009	T	2	Pd–(Ni–Zn)/C	Fe–CO K	55	20	10 W	–	Air	–
Bambagioni et al. [12], 2009	T	2	Pd/MWCNT	Fe–CO K	18	20	10 W	–	Air	–
Tadanaga et al. [18], 2010	H <sup>f</sup>	10 W	Ni–Co/C	Fe–CO/C	65	80	10 W	–	Air	–

<sup>a</sup> Tokuyama.<sup>b</sup> PBI/KOH.<sup>c</sup> K14 Hypermec™.<sup>d</sup> Weight percentage.<sup>e</sup> Fumasep FAA.<sup>f</sup> Natural (Hydrotalcite, Mg – Al·CO<sub>3</sub><sup>2-</sup>) clay.

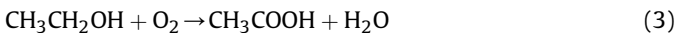
anode and cathode. A hydroxyl ion conductive membrane, AEM, separates the anode and cathode compartments. As depicted in Fig. 1, ethanol diffuses through the anode DL to reach the CL. Using the state-of-the-art catalyst, the full cleavage of a C–C bond in ethanol is nearly impossible. Many researchers reported that with the available catalyst, ethanol is only oxidized to acetic acid rather than CO<sub>2</sub> [6,21]. This is advantageous in terms of reducing the available CO<sub>2</sub> in the system and mitigating the carbonate precipitation, though an incomplete EOR lowers the system energy density. The EOR is:



While water is produced in the anode, it is required for the oxygen reduction reaction (ORR) in the cathode:



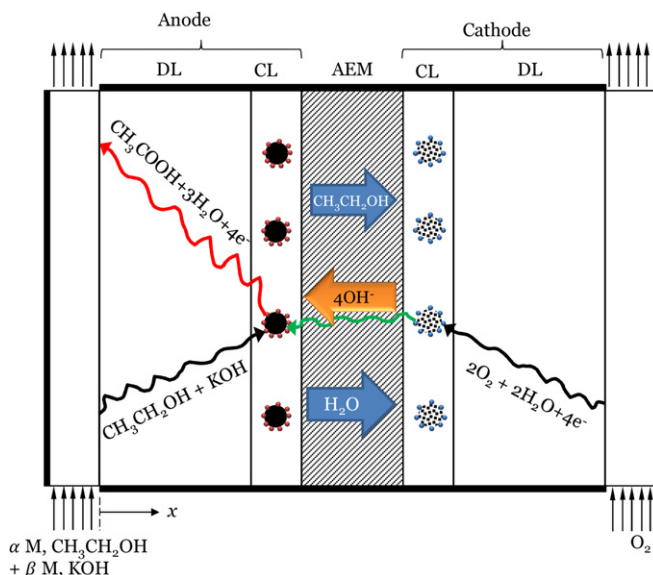
Electrons of Eq. (1) go through an external load and reach the cathode DL and CL. The hydroxyl ions of Eq. (2) pass through the AEM to reach the anode CL. The overall reaction is:



There are two mechanisms for ethanol transport through the membrane (crossover): (i) ethanol transfers through the membrane from the anode to cathode by the concentration gradient, the so-called diffusion, and (ii) ethanol also sticks to the hydroxyl ions (OH<sup>–</sup>) traveling through the membrane from the cathode CL to the anode CL, the so-called electroosmosis. Electroosmotic coefficient refers to the number of moles of ethanol attached to 1 mol of traveling OH<sup>–</sup> through the membrane.

In the remainder of this section, first, an analytical solution for the electrochemistry of an AEM-DEFC is provided. The closed form solution for two limiting cases of current density is obtained. The multi-layer membrane model is then presented to solve the mass transport. The following assumptions are made:

- Ethanol migrated from the anode to the cathode through the membrane will be completely oxidized in the cathode CL. Thus, the concentration of ethanol in the cathode is assumed zero.
- The effect of KOH on the kinetics of EOR as well as on the membrane ion conductivity is neglected.
- The membrane is impermeable to the gas phase.
- The electron conductivity of the carbon phase is infinity relative to the ion conductivity of the membrane phase.
- Diffusion and electroosmosis are two mechanisms of ethanol transport through the membrane.
- Water concentration in the anode is much higher than that of ethanol and KOH.
- The kinetics of ORR and EOR are approximated by Tafel expressions.

**Fig. 1.** A representative schematic of DEFC operation with an AEM.

- The concentration of ethanol and KOH in the anode channel and the concentration of oxidizer ( $O_2$ ) in the cathode channel are constant.
- Two phase flow in the cathode is neglected.
- Convective mass transport in the DL and CL is negligible.
- The flow is isothermal and one-dimensional. The change in transport variables is only considered in the  $x$ -direction.

### 2.1. Electrochemistry

In the following section, an analytical solution for the anode and cathode overpotentials is presented. The cell voltage for a given current density is then obtained. The procedure is similar to what was already provided for a passive DMFC [22,23]. The EOR rate ( $R_{ox}$ ,  $A m^{-3}$ ) in the anode CL is estimated by Tafel kinetics:

$$R_{ox} = J_{o,e}^{\text{ref}} \left( \frac{C_{e,a}^{\text{CL}}}{C_{e,a}^{\text{ref}}} \right)^{\gamma_a} \exp \left( \frac{\alpha_a \eta_a F}{R_u T} \right) \quad (4)$$

where subscripts  $a$ ,  $e$ , and  $ox$  denote anode, ethanol and oxidation, respectively, and superscripts  $CL$  and  $\text{ref}$  pertain to the catalyst layer and reference value.  $J_{o,e}^{\text{ref}}$  is the anode exchange current density ( $A m^{-3}$ ),  $\alpha$  is the transfer coefficient,  $\eta$  is overpotential (V),  $F$  is the Faraday's constant (96,485.3,  $A s mol^{-1}$ ),  $R_u$  is the universal gas constant ( $8.314, J mol^{-1} K^{-1}$ ),  $C$  is the concentration ( $mol m^{-3}$ ),  $T$  is the temperature (K), and  $\gamma_a$  determines whether the oxidation

reaction rate is zero or first order with respect to the ethanol concentration in the anode CL ( $C_{e,a}^{\text{CL}}$ ):

$$\gamma_a = \begin{cases} 0 & C_{e,a}^{\text{CL}} > C_{e,a}^{\text{ref}} \\ 1 & C_{e,a}^{\text{CL}} \leq C_{e,a}^{\text{ref}} \end{cases} \quad (5)$$

The anode overpotential is:

$$\eta_a = \phi_{car,a} - \phi_{mem} - U \quad (6)$$

where  $\phi$  is the phase potential (V),  $U$  is the equilibrium potential (V), and subscripts  $car$  and  $mem$  denote carbon and membrane phases, respectively. Note that either the electronic,  $I_e(x')$ , or anionic,  $I_{OH}(x')$ , current density may be employed to calculate overpotentials at the anode CL. However, since infinite electron conductivity for the carbon phase is assumed here, all the calculations are based on the anionic current density.

The anode CL depicted in Fig. 2(a) is the solution domain for the anode overpotential. Note that the  $x'$ -coordinate shown in this figure is different than  $x$ -coordinate in Fig. 1 which is for the mass transport calculation. The relations for the current density ( $I_{OH}$ ,  $A m^{-2}$ ) inside the anode CL are:

$$\begin{cases} \frac{dI_{OH}}{dx'} = -R_{ox} & 0 \leq x' \leq L_{a,CL} \\ I_{OH} = -\sigma_{mem} \frac{d\phi_{mem}}{dx'} \end{cases} \quad (7)$$

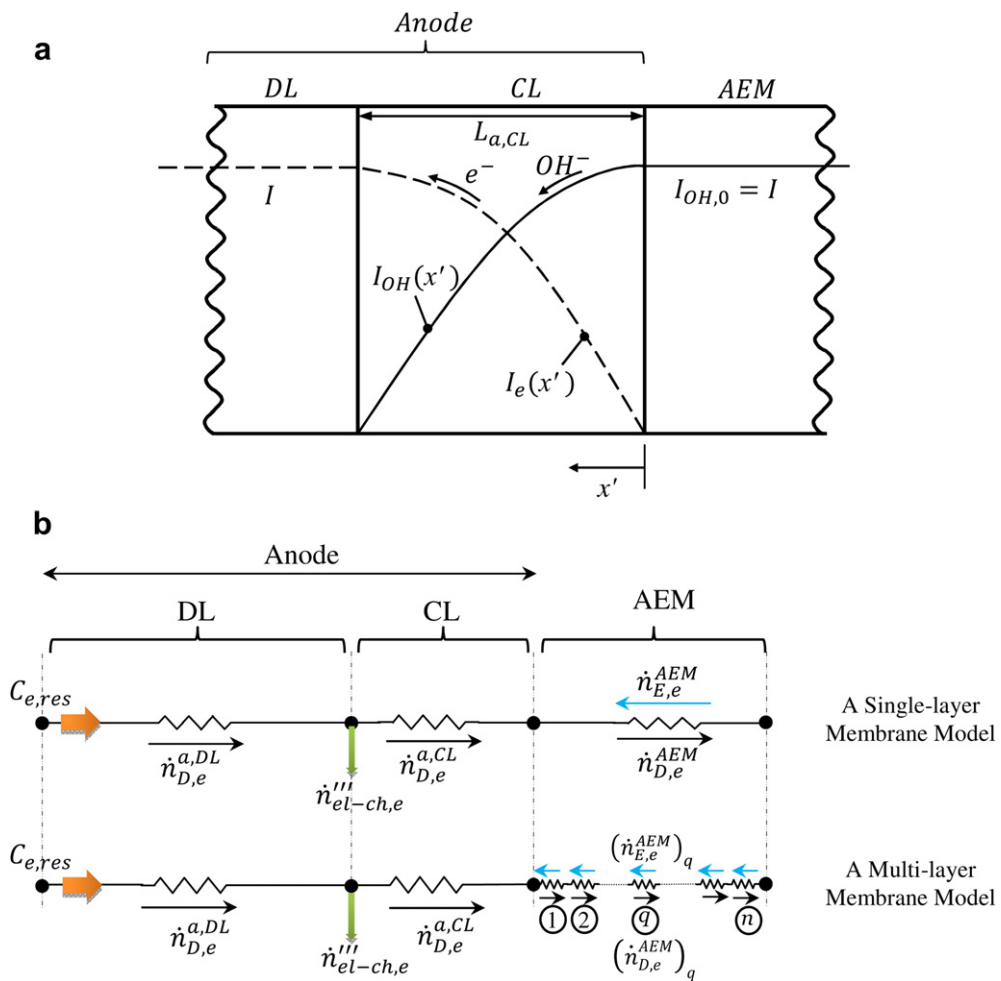


Fig. 2. A representative schematic of (a) anionic,  $I_{OH}(x')$ , and electronic,  $I_e(x')$ , current densities in the anode and membrane, and (b) single-layer and multi-layer membrane models.

where  $\sigma$  is anion conductivity of the membrane phase inside the anode CL ( $\Omega^{-1} \text{m}^{-1}$ ).

The pertinent dimensionless parameters are:

$$\bar{x}' = \frac{x'}{L_{a,CL}}, \quad \bar{I}_{OH} = \frac{I_{OH}}{I_{OH,a}^*}, \quad \bar{\eta} = \frac{\eta}{\eta_a^*}, \quad \bar{R}_{ox} = \frac{R_{ox}}{R_a^*} \quad (8)$$

where subscript CL pertains to catalyst layer and the starred values are:

$$I_{OH,a}^* = \frac{2\sigma_{mem}R_uT}{\alpha_aFL_{a,CL}}, \quad \eta_a^* = \frac{R_uT}{\alpha_aF}, \quad R_a^* = \frac{I_{OH,a}^*}{L_{a,CL}} \quad (9)$$

Upon combining Eqs. (4) and (6) into Eq. (7) and utilizing the dimensionless parameters of Eqs. (8) and (9), the current density inside the anode CL becomes:

$$\frac{d^2\bar{I}_{OH}}{dx'^2} + \frac{d\bar{I}_{OH}}{dx'} = 0 \quad (10)$$

Eq. (10) is solved in the following conservative form:

$$\frac{d\bar{I}_{OH}}{dx'} + \bar{I}_{OH}^2(\bar{x}') = -\bar{R}_{ox}(\bar{x}') + \bar{I}_{OH}^2(\bar{x}') = -\bar{R}_{ox,0} + \bar{I}_{OH,0}^2 = \text{cons} \quad (11)$$

where subscript 0 denotes  $x' = 0$  in Fig. 2(a) and  $I_{OH,0}$  is the cell current density. The constant value in Eq. (11) must be negative for a physical solution. Eq. (11) is solved for  $\bar{I}_{OH}(\bar{x}')$ . Upon using the condition of  $\bar{I}_{OH}(\bar{x}') = 0$  at  $\bar{x}' = 1$ , the dimensionless cell current density (at  $x' = 0$ ) is expressed as:

$$\bar{I}_{OH,0} = \sqrt{\bar{R}_{ox,0} - \bar{I}_{OH,0}^2} \cdot \tan\left(\sqrt{\bar{R}_{ox,0} - \bar{I}_{OH,0}^2}\right) \quad (12)$$

There is no closed-form solution for  $\bar{I}_{OH,0}$  in Eq. (12). However, the solution is obtained for two limiting cases:

- $\bar{I}_{OH,0} \ll 1$ : the right hand side of Eq. (12) is small. For  $0 < \beta \cdot \tan(\beta) \ll 1$ , it may be concluded that  $\tan(\beta) \ll 1$ . Eq. (12) is then approximated as  $\bar{I}_{OH,0} \approx \bar{R}_{ox,0} - \bar{I}_{OH,0}^2$ . Neglecting  $\bar{I}_{OH,0}^2$  compared to  $\bar{I}_{OH,0}$ , the final expression is further simplified as  $\bar{I}_{OH,0} \approx \bar{R}_{ox,0}$ . Considering the typical conditions of  $T \approx 300 \text{ K}$ ,  $\sigma_{mem} \approx 3 \Omega^{-1} \text{m}^{-1}$ ,  $L_{a,CL} \approx 0.02 \text{ mm}$ , and  $\alpha_a \approx 1$ , the  $I_{OH,a}^*$  will be  $\approx 7755 \text{ A m}^{-2}$ . Thus, the above-noted approximation is valid for a wide range of practical current density in DEFCs, that is  $0 \leq I_{OH,0} \lesssim 700 \text{ A m}^{-2}$ .
- $\bar{I}_{OH,0} \gg 1$ : it is assumed that due to a very large value of  $\bar{I}_{OH,0}$ ,  $(\bar{R}_{ox,0} - \bar{I}_{OH,0}^2) \rightarrow \pi^2/4$ . Neglecting  $\pi^2/4$  compared to  $\bar{I}_{OH,0}^2$ , Eq. (12) is simplified to  $\bar{I}_{OH,0} \approx (\bar{R}_{ox,0})^{0.5}$ . Followed by the preceding discussion, utilizing Eqs. (4) and (8), the anode overpotential is obtained as:

$$\bar{\eta}_{a,0} \approx \begin{cases} \ln(\bar{I}_{OH,0}) - \ln(\tilde{R}_{ox}/R_a^*) & \bar{I}_{OH,0} \ll 1 \\ 2\ln(\bar{I}_{OH,0}) - \ln(\tilde{R}_{ox}/R_a^*) & \bar{I}_{OH,0} \gg 1 \end{cases} \quad (13)$$

where  $\tilde{R}_{ox}$  is  $R_{ox}$  of Eq. (4) when  $\eta_a = 0$ . Eq. (13) is roughly generalized for the whole range of  $\bar{I}_{OH,0}$ , as follows [23]:

$$\bar{\eta}_{a,0} \approx \varphi(\bar{I}_{OH,0}) \cdot \ln(\bar{I}_{OH,0}) - \ln(\tilde{R}_{ox}/R_a^*) \quad (14)$$

where

$$\varphi(\bar{I}_{OH,0}) = \frac{1 + 2\bar{I}_{OH,0}}{1 + \bar{I}_{OH,0}} \quad (15)$$

Attention is now directed to the cathode overpotential. Similar to the anode side, the ORR rate in the cathode is approximated by Tafel kinetics:

$$R_{red} = J_{O_2,O_2}^{\text{ref}} \left( \frac{C_{O_2,c}^{\text{CL}}}{C_{O_2,c}^{\text{ref}}} \right)^{\gamma_c} \exp\left(\frac{\alpha_c \eta_c F}{R_u T}\right) \quad (16)$$

where subscripts red,  $O_2$  and  $c$  denote reduction, oxygen and cathode, respectively. The variable  $\gamma_c$  determines whether the ORR rate is zero or first order with respect to  $C_{O_2,c}^{\text{CL}}$ :

$$\gamma_c = \begin{cases} 0 & C_{O_2,c}^{\text{CL}} > C_{O_2,c}^{\text{ref}} \\ 1 & C_{O_2,c}^{\text{CL}} \leq C_{O_2,c}^{\text{ref}} \end{cases} \quad (17)$$

The cathode overpotential is:

$$\eta_c = \phi_{car,c} - \phi_{mem} - U_{O_2} \quad (18)$$

Taking a similar procedure as Eqs. (7)–(13), the cathode overpotential is calculated as:

$$\bar{\eta}_{c,0} \approx \varphi(\bar{I}_{OH,0}) \cdot \ln(\bar{I}_{OH,0}) - \ln(\tilde{R}_{red}/R_c^*) \quad (19)$$

where  $\tilde{R}_{red}$  is  $R_{red}$  of Eq. (16) when  $\eta_c = 0$ . Note that for the ORR, the origin of the coordinate,  $x'' = 0$ , starts at the interface of the membrane and cathode CL towards the interface of the cathode CL and DL. The pertinent dimensionless parameters for the cathode are:

$$\bar{x}'' = \frac{x''}{L_{c,CL}}, \quad \bar{I}_{OH} = \frac{\bar{I}_{OH,0}}{I_{OH,c}^*}, \quad \bar{\eta} = \frac{\eta}{\eta_c^*}, \quad \bar{R}_{red} = \frac{R_{red}}{R_c^*} \quad (20)$$

where

$$I_{OH,c}^* = \frac{2\sigma_{mem}R_uT}{\alpha_cFL_{c,CL}}, \quad \eta_c^* = \frac{R_uT}{\alpha_cF}, \quad R_c^* = \frac{I_{OH,c}^*}{L_{c,CL}} \quad (21)$$

In the remaining sections, for the sake of simplicity,  $I_{OH,0}$  is replaced by  $I$  denoting the cell current density.

The effect of ethanol crossover ( $\dot{n}_{cr,e}''$ ,  $\text{mol} \cdot \text{m}^{-2} \text{s}^{-1}$ ) on the cathode overpotential is also considered. The preliminary crossover predictions show that parasitic current density,  $I_p = 4F \cdot \dot{n}_{cr,e}''$ , is small compared to the cell current density in AEM-DEFCs with  $C_{e,res} \leq 3 \text{ M}$ . Assuming no mass transport limit for oxygen and ethanol in the cathode CL, Butler–Volmer relation can be linearized as follows [24]:

$$\eta_{p,e,c} = \frac{I_p/L_{c,CL}}{J_{O,e}^{\text{ref}} \cdot 4F}, \quad \eta_{p,O_2,c} = \frac{I_p/L_{c,CL}}{J_{O,O_2}^{\text{ref}} \cdot 4F} \quad (22a)$$

$$\eta_c^{eff} = \eta_c + \eta_{p,e,c} + \eta_{p,O_2,c} \quad (22b)$$

where  $\eta_{p,e,c}$  and  $\eta_{p,O_2,c}$  denote the cathode overpotentials due to the reacted ethanol in the cathode CL and the corresponding oxygen reduction, respectively. Cell voltage ( $V_{cell}$ ), by definition, is the difference between the carbon phase potential of the anode ( $\phi_{car,a}$ ) and the cathode ( $\phi_{car,c}$ ):

$$V_{cell} = \phi_{car,c} - \phi_{car,a} \quad (23)$$

Anions flowing through the membrane encounter internal resistance ( $R_{r,mem}$ ) which causes a potential drop in membrane phase potential ( $\phi_{mem}$ ):

$$R_{r,mem} = \frac{\phi_{mem,a} - \phi_{mem,c}}{I} = \frac{L_{AEM}}{\sigma_{mem}} \quad (24)$$

Cell potential is presented as [22]:

$$V_{cell} = (U_{O_2} - U_e) - \eta_a - \eta_c^{eff} - I \left( R_{con} + \frac{L_{AEM}}{\sigma_{mem}} \right) \quad (25)$$

where  $R_{con}$  is the contact resistance and  $E_{rev} = (U_{O_2} - U_e)$  represents the reversible cell voltage.  $E_{rev}$  is calculated as:

$$E_{rev} = -\frac{\Delta G}{4F} = -\frac{\Delta H - T \Delta S}{4F} \quad (26)$$

where  $\Delta G$  is the change in the Gibbs free energy of the overall reaction of Eq. (3). At standard conditions,  $E_{rev} = 1.167$  V. Van't Hoff relation is employed to find the equilibrium potential as a function of temperature. The change in Gibbs energy when the temperature changes from  $T_o$  to  $T$  is [25]:

$$\frac{\Delta G}{T} = \frac{\Delta G_o}{T_o} + \Delta H_o \left( \frac{1}{T} - \frac{1}{T_o} \right) \quad (27)$$

Assuming  $T_o = 298$  K, the equilibrium potential as a function of temperature is:

$$E_{rev} = 1.167 - 3.59 \times 10^{-4}(T - 298) \quad (28)$$

## 2.2. Mass transport

Eqs. (14) and (19) require ethanol and oxygen concentrations in the CLs. Mass transport in a DEFC is similar to that in a DMFC except that the electroosmotic transport in an AEM is from the cathode to anode. Several one-dimensional, analytical models for the mass transport in a DMFC are reported, all of which considered the membrane as a single layer. Representative examples are [22,26,27]. As will be evident, a single-layer model for the AEM results in a non-physical prediction of ethanol transport through the membrane.

In order to provide an appropriate model for the ethanol transport through the membrane, a multi-layer membrane model is proposed in this study. Fig. 2(b) illustrates the difference between a single-layer and a multi-layer membrane model. Variables  $\dot{n}_{D,e}''$  and  $\dot{n}_{E,e}''$  denote the diffusive and electroosmotic flux of ethanol, respectively:

$$\dot{n}_{D,e}'' = -D_e^{eff} \frac{dC_e}{dx} \quad (29)$$

$$\dot{n}_{E,e}'' = n_{d,e} \frac{I}{4F} \quad (30)$$

where  $dC_e/dx$  is the gradient of ethanol concentration within each representative layer (resistance) shown in Fig. 2(b) and  $n_{d,e}$  is the electroosmotic drag coefficient of ethanol:

$$n_{d,e} = n_d \cdot x_e \quad (31)$$

where  $n_d$  is the electroosmotic drag coefficient of liquid within the membrane and  $x_e$  denotes the local ethanol mole fraction. The electrochemical mass consumption of ethanol in the anode CL,  $\dot{n}_{el-ch,e}'''$ , is:

$$\dot{n}_{el-ch,e}''' = \frac{I}{4F \cdot L_{a,CL}} \quad (32)$$

Oxygen mass transport in the cathode is similarly solved, noting that the membrane is impermeable to the oxygen. The electrochemical oxygen consumption in the cathode CL  $\dot{n}_{el-ch,o_2}'''$ , accounts for both the electrons from the external load and the crossover flux of ethanol through the membrane,  $\dot{n}_{cr,e}''$ :

$$\dot{n}_{el-ch,o_2}''' = \frac{I}{4F \cdot L_{c,CL}} + \frac{\dot{n}_{cr,e}''}{L_{c,CL}} \quad (33)$$

The effective diffusivity coefficient is calculated accounting for the porosity,  $\epsilon$ , and the liquid saturation,  $s$ , as:

$$D_e^{eff} = \begin{cases} D_e \cdot (\epsilon \cdot s_a)^{1.5} & \text{anode CL, DL} \\ D_{e,mem} \cdot \epsilon_{mem}^{1.5} & \text{AEM} \end{cases} \quad (34)$$

$$D_{O_2}^{eff} = D_{O_2} \cdot (\epsilon \cdot (1 - s_c))^{1.5} \quad (35)$$

## 3. Solution methodology and properties

Solving Eqs. (29)–(33) provides the local distribution of ethanol and oxygen concentrations. For  $n$  layers (resistances) in the membrane,  $m$  in the anode CL and  $k$  in the anode DL,  $n + m + k - 1$  mass conservation equations form a well-posed description of ethanol concentration in the anode. The electrochemical ethanol consumption in the anode CL is uniformly distributed to the all  $m$  layers in the anode CL. An iterative procedure is required to solve the linear algebraic equation since the electroosmotic drag of ethanol depends on the ethanol molar fraction (Eq. (31)). A TDMA solver is developed to solve the linear equations. The iteration for the final converged results is checked for the maximum local error criterion:

$$\max |\psi_j^{i+1} - \psi_j^i| < 10^{-12} \quad (36)$$

where  $i$  denotes the iteration number, and  $\psi_j$  is the flow variable at cell  $j$ .

Distribution of oxygen concentration in the cathode is obtained in a similar fashion as the ethanol in the anode. Pure oxygen and a constant concentration of ethanol in the cathode and anode channels are respectively assumed. The ethanol concentration in the cathode is zero. Membrane is supposed to be impermeable to the oxygen. The converged solutions of oxygen and methanol concentrations are used to obtain the cell voltage using Eqs. (14), (19) and (25).

As will be evident, for  $n_{AEM} \geq 16$ , the ethanol crossover prediction becomes independent of the number of layers in the membrane. Unless otherwise noted, all the predictions in this study are for  $n_{AEM} = 32$ ,  $n_{a,CL} = 5$ ,  $n_{a,DL} = 2$ ,  $n_{c,CL} = 5$  and  $n_{c,DL} = 2$ .

Properties of AEMs are not well established yet, due in part to the diversity of utilized AEMs for DEFC applications. There are few studies available regarding the measurement of transport properties in AEMs including the diffusivity coefficient of ethanol through the membrane [7,19,28,29] and the electroosmotic drag coefficient [19,30]. Table 2 presents the measured diffusivity coefficient of ethanol ranging from  $8.6 \times 10^{-12}$  to  $6.5 \times 10^{-11} \text{ m}^2 \text{s}^{-1}$  for various AEMs. Note that the table emphasizes another distinct advantage of AEM-DEFCs over DMFCs in two respects: (i) ethanol diffuses less than methanol in any transport medium due to its larger molecular structure, and (ii) nearly all the common AEMs exhibit lower diffusivity coefficient than Nafion no matter what kind of fuel is utilized [28]. The physicochemical properties, cell geometries and operating conditions utilized in this study are provided in Tables 3 and 4, respectively.

**Table 2**  
Diffusivity coefficient of ethanol in various AEMs.

Type of AEM	$D_{e,mem} (\text{m}^2 \text{s}^{-1})$	Investigator
Tokuyama	$2 \times 10^{-11}$	Varcoe et al. [28]
PBI/KOH	$6.5 \times 10^{-11}$	Hou et al. [7]
	$8.6 \times 10^{-12}$	Leykin et al. [19]
PVA/TiO <sub>2</sub> composite polymer	$2.81 \times 10^{-11}$	Yang et al. [29]

**Table 3**  
Physicochemical properties.

Parameters	Symbol	Value	Unit	Ref.
Diffusivities, ethanol	$D_e$	$(-5.7939x_e^3 + 11.696x_e^2 - 6.1678x_e + 1.3679) \times 10^{-9}$	$\text{m}^2 \text{s}^{-1}$	[31]
Diffusivity in the membrane, ethanol	$D_{e,mem}$	$1. \times 10^{-11}$	$\text{m}^2 \text{s}^{-1}$	[7,19,28,29]
Diffusivities, oxygen	$D_{O_2}$	$1.775 \times 10^{-5}(T/273.15)^{1.823}$	$\text{m}^2 \text{s}^{-1}$	[32]
Ion conductivity of the membrane	$\sigma_{mem}$	$3 + 2.57 \cdot (T - 303) 10^{-2}$	$\Omega^{-1} \text{m}^{-1}$	[33]
Electro-osmotic drag coefficient	$n_d$	$2.3 + 0.13 \cdot (T - 303)$	—	[30]
Anode transfer coefficient	$\alpha_a$	0.27	—	Fitted
Cathode transfer coefficient	$\alpha_c$	0.27	—	Fitted
Anode exchange current density	$J_{O_2,e}^{ref}$	$2.5 \times 10^5$	$\text{A m}^{-3}$	Fitted
Cathode exchange current density	$J_{O_2,O}^{ref}$	$2.2 \times 10^5$	$\text{A m}^{-3}$	Fitted
Anode reference concentration	$C_{e,a}^{ref}$	100	$\text{mol m}^{-3}$	Assumed
Cathode reference concentration	$C_{O_2,c}^{ref}$	40.9	$\text{mol m}^{-3}$	Assumed
Liquid water density	$\rho_{H_2O}$	1000.0	$\text{Kg m}^{-3}$	[34,35]
Liquid ethanol density	$\rho_{ke}$	789.0	$\text{Kg m}^{-3}$	
Contact Resistance	$R_{con}$	$3 \times 10^{-5}$	$\Omega \text{m}^2$	Measured for a DMFC
Absolute entropy (1 atm, 298 K)	Liquid phase	$\bar{s}_{CH_3COOH}$ $\bar{s}_{H_2O}$ $\bar{s}_e$	$\text{J mol}^{-1} \text{K}^{-1}$ $\text{J mol}^{-1} \text{K}^{-1}$ $\text{J mol}^{-1} \text{K}^{-1}$	
Enthalpy of formation (1 atm, 298 K)	Gas phase	$\bar{s}_{O_2}$	$\text{J mol}^{-1} \text{K}^{-1}$	[34,35]
	Liquid phase	$\bar{h}_{CH_3COOH}$ $\bar{h}_{H_2O}$ $\bar{h}_e$	$\text{J mol}^{-1}$ $\text{J mol}^{-1}$ $\text{J mol}^{-1}$	
	Gas phase	$\bar{h}_{O_2}$	$\text{J mol}^{-1}$	

#### 4. Results

The proposed model was calibrated, to the extent possible, by predicting the experimentally measured values of the cell voltage and power density [10]. Fig. 3 presents a comparison of the cell voltage solution of Eq. (25) to the polarization curve and the power density of [10] when  $C_{e,res} = 1 \text{ M}$  and pure oxygen is fed to the cathode channel. The cell temperature is  $T = 303 \text{ K}$ . A good agreement is observed between the numerical predictions and the experimental data.

##### 4.1. Electroosmotic drag coefficients

The focus of this section is to emphasize the differences in mass transport within the membrane corresponding to the positive and negative electroosmotic drag coefficients. Electroosmotic transport of one species in the membrane linearly scales with the local mole fraction of that species, Eqs. (30) and (31). In most DMFC models developed so far, as a typical system in which the electroosmotic drag coefficient is positive, the membrane is considered a single layer and the electroosmotic transport of methanol is modeled based on the concentration of methanol at the interface of the anode CL and membrane [22,36–42]. This approach works properly for DMFCs where the directions of both electroosmotic and

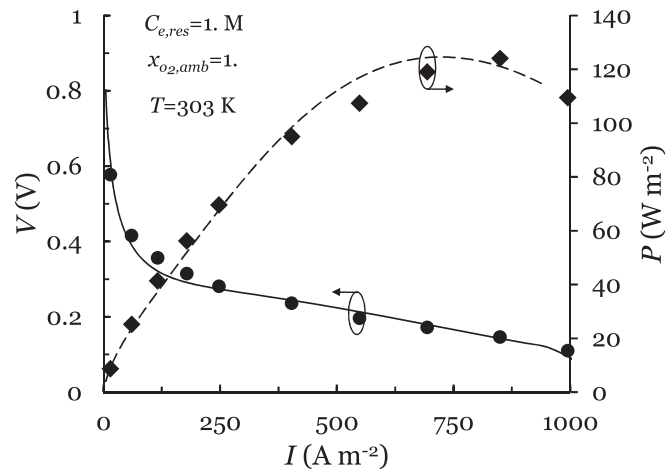


Fig. 3. Comparison of the prediction of Eq. (24) to the experimentally measured values of the cell voltage and power density [10].

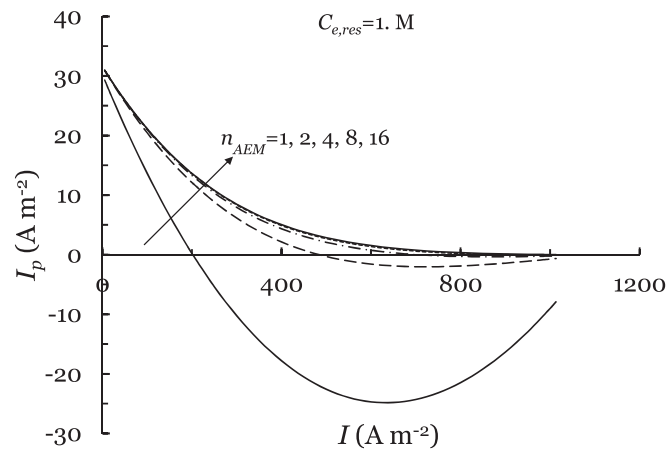
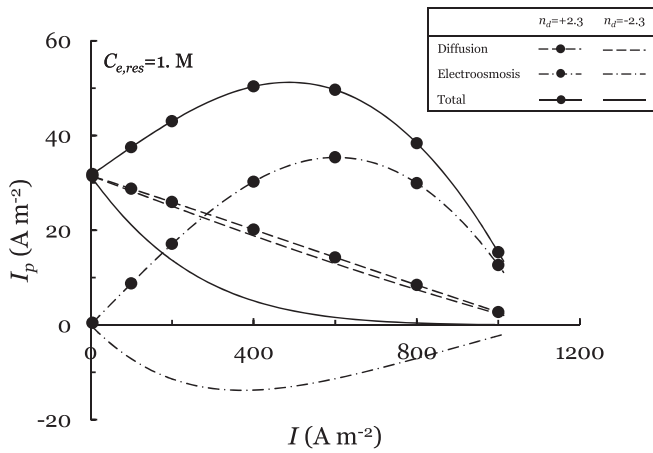


Fig. 4. Ethanol crossover prediction ( $I_p$ ) versus current density by employing the conventional, single-layer membrane model ( $n_{AEM} = 1$ ) compared to the multi-layer membrane model ( $n_{AEM} = 2, 4, 8, 16$ ).

**Table 4**  
Cell geometric dimensions and operating parameters.

Parameters	Symbols	Value	Unit
Anode DL thickness	$L_{a,DL}$	0.26	mm
Anode CL thickness	$L_{a,CL}$	0.02	mm
Membrane thickness	$L_{AEM}$	0.03	mm
Cathode CL thickness	$L_{C,CL}$	0.02	mm
Cathode DL thickness	$L_{C,DL}$	0.26	mm
Porosity of DL and CL	$\epsilon$	0.7	—
Porosity of membrane	$\epsilon_{mem}$	0.4	—
Cell temperature	$T$	303	K
Anode liquid saturation	$s_a$	1.0	—
Cathode liquid saturation	$s_c$	0.02	—



**Fig. 5.** The effect of positive and negative electroosmotic drag coefficients on the various ethanol crossover mechanisms as well as the total crossover,  $0 < I \leq 1000 \text{ A m}^{-2}$ .

diffusive transport are from the anode to the cathode. However, for a fuel cell system employing an AEM where the electroosmotic transport is negative (from the cathode to anode) following the similar procedure fails and results in a non-physical prediction of ethanol crossover.

In an AEM-DEFC, the electroosmotic mechanism operates in the opposite direction of the diffusion. The net mass flux of ethanol is

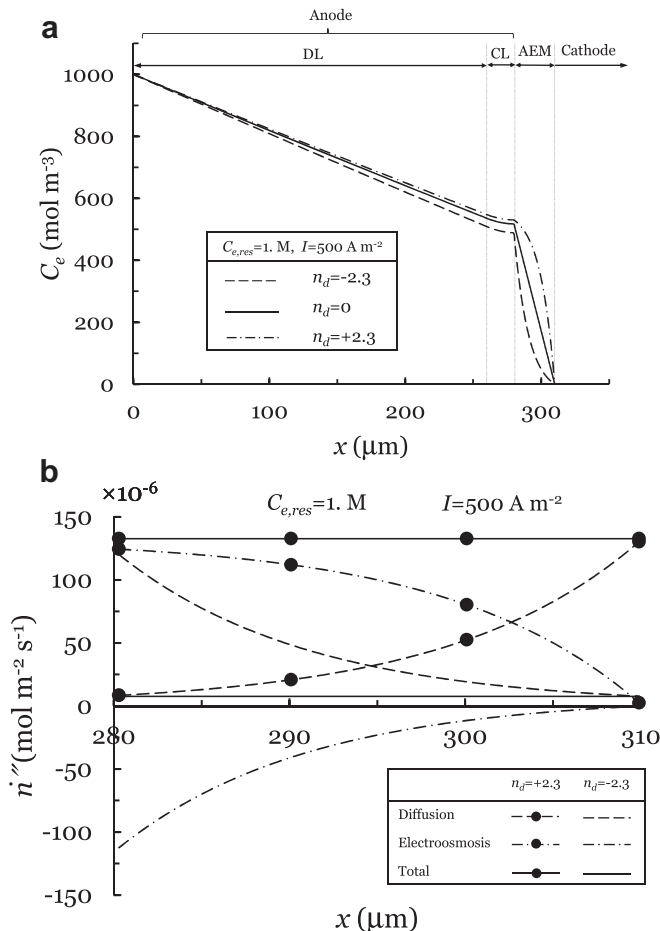


**Fig. 6.** The effect of positive and negative electroosmotic drag coefficients (a) on the ethanol distribution in the anode and membrane, and (b) on the various ethanol crossover mechanisms within the membrane, when  $C_{e,res} = 1 \text{ M}$  and  $I = 500 \text{ A m}^{-2}$ .

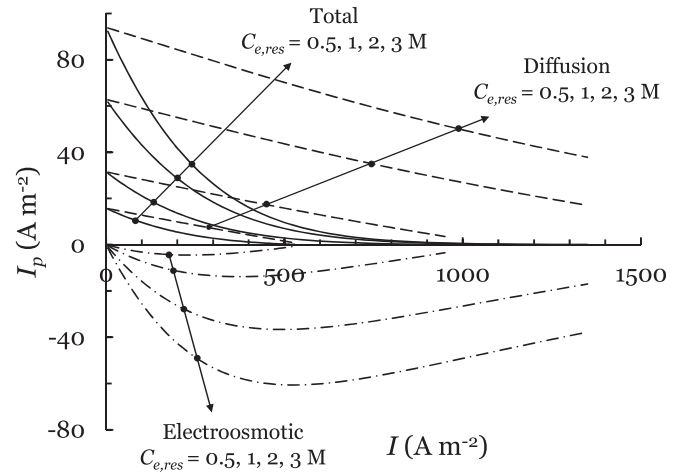


**Fig. 7.** Diffusive (dashed line), electroosmotic (dashed-dot line), and total (continuous line) ethanol crossover through an AEM, when  $C_{e,res}$  is 0.5, 1, 2, and 3 M.

therefore obtained by subtracting the electroosmotic transport from the diffusive transport (Fig. 2(b)). An appropriate number of layers in the membrane is required to get a physical predictions of the ethanol transport through the membrane. Since the ethanol is

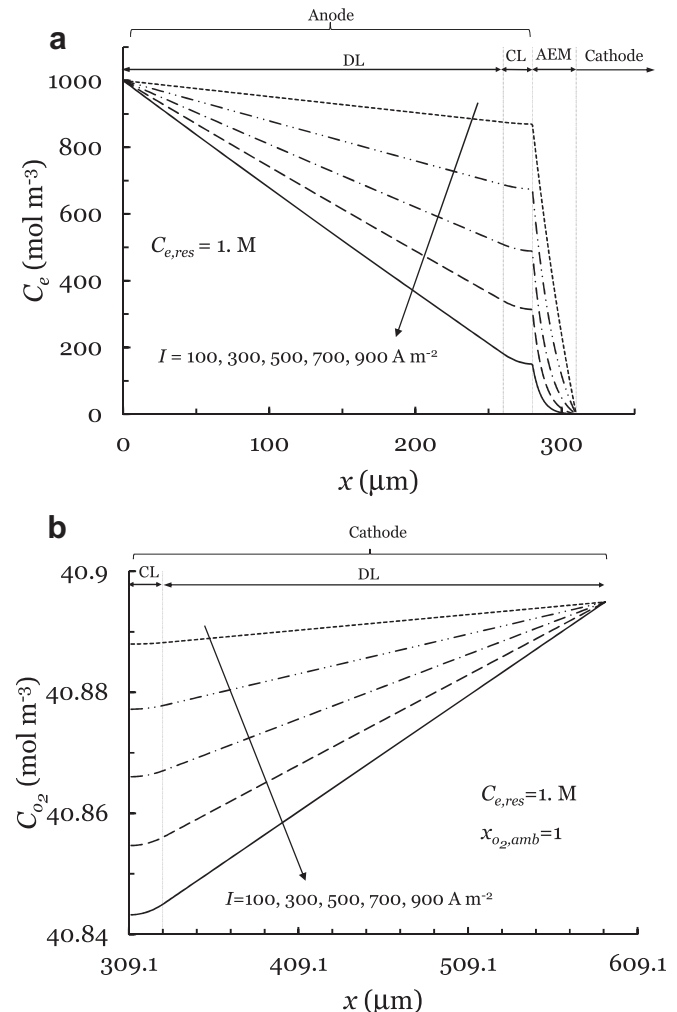


**Fig. 8.** Local distribution of (a) the ethanol concentration in the anode and the membrane, and (b) the oxygen concentration in the cathode, for various values of current density.

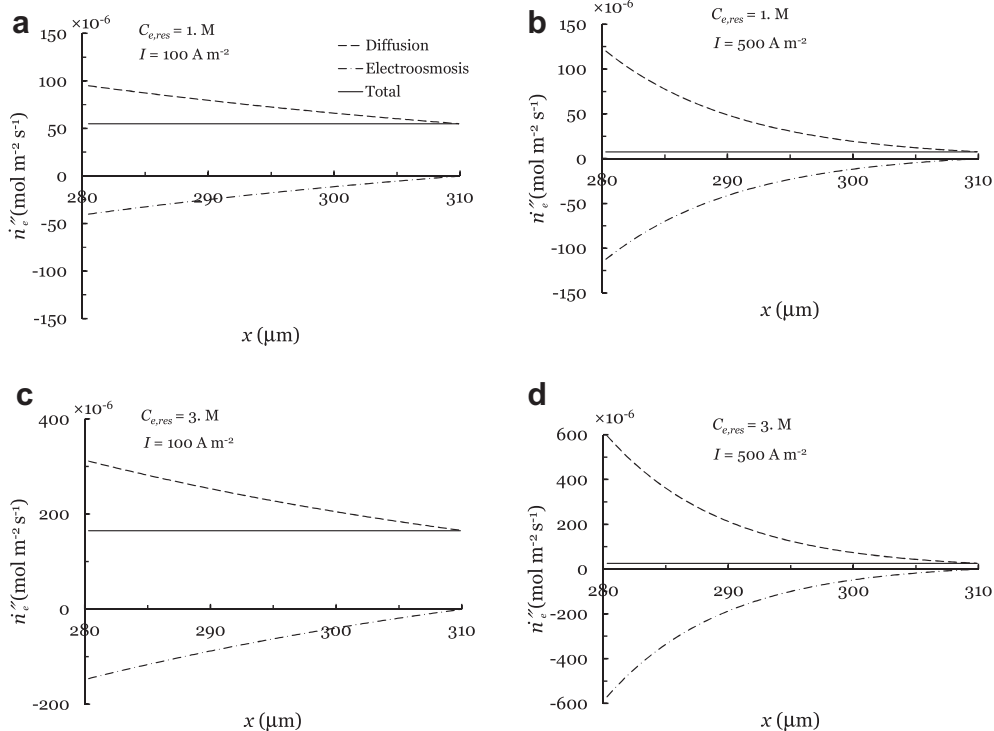


**Fig. 9.** Local distribution of the diffusive (dashed line), electroosmotic (dashed-dot line), and total (continuous line) ethanol flux in the membrane of an AEM-DEFC, when  $C_{e,res}$  and  $I$  are respectively: (a) 1 M and  $100 \text{ A m}^{-2}$ , (b) 1 M and  $500 \text{ A m}^{-2}$ , (c) 3 M and  $100 \text{ A m}^{-2}$ , and (d) 3 M and  $500 \text{ A m}^{-2}$ .

supplied in the anode, the negative ethanol crossover is not a physical solution. Fig. 4 delineates the predictions of the ethanol crossover through the membrane for various selected number of layers in the membrane,  $n_{AEM}$ , when  $n_{a,CL} = 5$ ,  $n_{a,DL} = 2$  and  $C_{e,res} = 1 \text{ M}$ . The conventional one-layer membrane model, represented by  $n_{AEM} = 1$ , results in a negative ethanol crossover at medium and high current densities. Increasing the number of layers in the membrane mitigates the nonphysical, negative ethanol crossover and, as evident, the predictions become grid independent for  $n_{AEM} > 16$ .

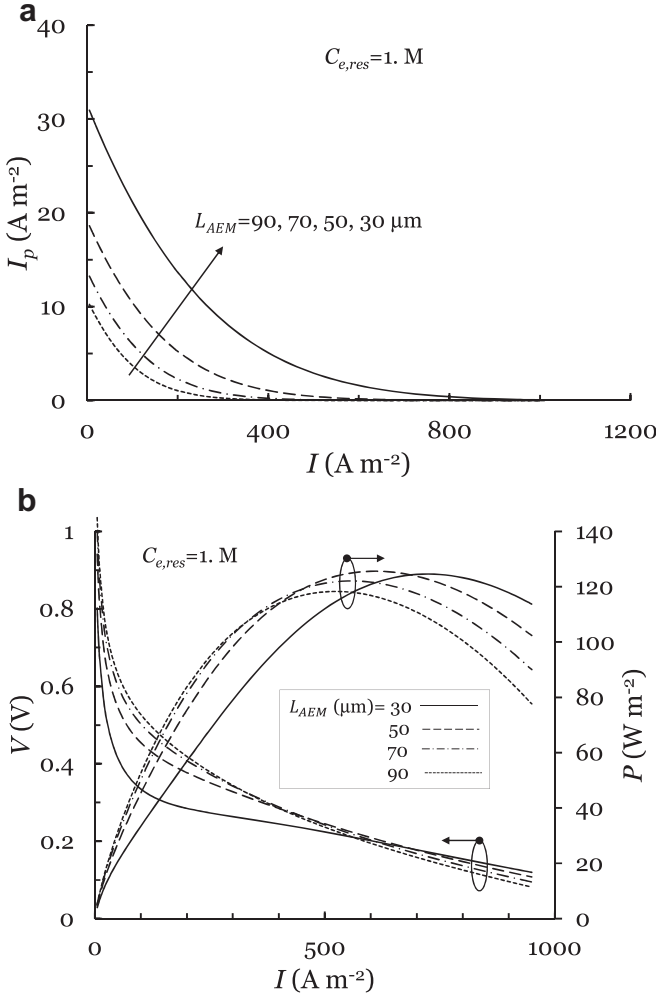
Fig. 5 delineates the difference between various ethanol crossover mechanisms, and the total crossover in a DEFC for the positive and negative electroosmotic drag coefficients ( $n_d$ ). The positive  $n_d$  represents a DEFC using a proton exchange membrane. All conditions are identical for two cases of positive and negative  $n_d$ . Reported values are averaged. While the difference in the diffusive transport for two cases of negative and positive  $n_d$  is nearly negligible, a significant difference is observed in electroosmotic transport and the total crossover. The trend of predicted total crossover for the positive  $n_d$  case shows a good agreement with the trend of both experimental measurements [4] and numerical predictions [43,44] of methanol crossover in a DMFC, a representative of a system with  $n_d > 0$ .

Fig. 6 illustrates the influence of the change in electroosmotic drag coefficient on the local distribution of ethanol concentration in the anode and membrane and the local ethanol flux within the membrane, when  $C_{e,res} = 1 \text{ M}$  and  $I = 500 \text{ A m}^{-2}$ . Fig. 6(a) shows the difference between the ethanol concentration distribution in the anode and the membrane for positive, negative and zero electroosmotic drag coefficients. It is observed that the greatest difference in ethanol concentration occurs within the membrane. While Fig. 5 demonstrates that the averaged value of diffusive transport of ethanol in the membrane is nearly identical for the positive and negative  $n_d$ , Fig. 6(a) delineates that the local diffusive transport of ethanol within the membrane should significantly be

different for various values of  $n_d$ . For  $n_d > 0$ , the gradient of ethanol concentration,  $dC_e/dx$ , varies from a near zero value at the interface of CL and AEM to a large value at the interface of the AEM and cathode. When  $n_d < 0$ ,  $dC_e/dx$  within the membrane decreases as  $x$  increases. Fig. 6(b) depicts the local diffusive, electroosmotic and total ethanol flux within the membrane for the positive and negative  $n_d$ . As evident, the diffusive flux of ethanol for  $n_d > 0$  is maximum where it is minimum for  $n_d < 0$ , and vice versa. The magnitude of electroosmotic fluxes for both positive and negative  $n_d$  nearly follow the same trend, and change from a maximum value at  $x = 280 \mu\text{m}$  to zero at  $x = 310 \mu\text{m}$ . The electroosmotic drag within the membrane is a function of ethanol concentration. A significant difference between the net flux of ethanol in the membrane is observed for two cases of positive and negative  $n_d$ . The net ethanol flux is  $132.7 \times 10^{-6} \text{ mol m}^{-2}\text{s}^{-1}$  for  $n_d = 2.3$ , whereas it drops to  $7.5 \times 10^{-6} \text{ mol m}^{-2}\text{s}^{-1}$  for  $n_d = -2.3$ .

#### 4.2. Mass transport in AEM-DEFCs

Attention is now directed to the AEM-DEFCs where  $n_d < 0$ . Fig. 7 displays averaged values for diffusive, electroosmotic and total ethanol crossover through the membrane, when  $0.5 \leq C_{e,res} \leq 3 \text{ M}$ . Diffusive crossover of ethanol monotonically decreases with increasing current density. It is increasing for higher concentration of ethanol in the anode reservoir. Electroosmotic crossover of ethanol from the cathode to anode is zero where  $I = 0$ . It increases to a maximum value due to the increasing current density and then starts to decrease to a minimum at  $I \approx I_{lim}$  owing to the low concentration of ethanol. Electroosmotic crossover is also increasing as more concentrated ethanol is fed to the anode. For all four cases shown in Fig. 7, the net ethanol crossover significantly decreases from the maximum value at  $I = 0$  to a near zero value at  $I \geq 500 \text{ A m}^{-2}$ . Reduction in ethanol crossover is the unique feature of an AEM-DEFC.



**Fig. 10.** The effect of increasing the membrane thickness on the (a) ethanol crossover and (b) cell polarization curve, when  $C_{e,res} = 1$  M.

**Fig. 8** delineates the local distribution of ethanol in the anode and membrane as well as the distribution of oxygen in the cathode, for  $100 \leq I \leq 900$  A m<sup>-2</sup> and  $C_{e,res} = 1$  M. As expected, both ethanol and oxygen concentrations decrease as current density increases. An initial increase and then a decrease in the electroosmotic drag of ethanol from the cathode to anode in **Fig. 7** is adequately explained through the ethanol distribution in the membrane. Electroosmotic drag is zero when  $I = 0$  and increases for increasing  $I$  (Eq. (30)). However,  $C_e$  in the membrane reduces as  $I$  increases, which in turn decreases the electroosmotic drag coefficient, according to Eq. (31). Electroosmotic drag from the cathode to the anode is minimum at  $I \approx I_{lim}$  due to the depletion of membrane from ethanol (**Fig. 8(a)**). Compared to **Fig. 8(a)**, **Fig. 8(b)** depicts that the oxygen concentration in the cathode never falls below the range that causes mass transport limitations.

**Fig. 9** shows the local electroosmotic and diffusive fluxes of ethanol within the membrane, when  $I = 100, 500$  A m<sup>-2</sup> and  $C_{e,res} = 1, 3$  M. Electroosmotic flux of ethanol from the cathode to anode is maximum at  $x = 280$  μm, where the  $C_e$  has the highest value in the membrane. It is zero at  $x = 310$  μm, where it is assumed that the concentration of ethanol is zero. The local diffusive transport of ethanol also starts from a maximum at  $x = 280$  μm, and ends at a value equal to the net total flux of ethanol at  $x = 310$  μm. As evident, the local magnitude of electroosmotic flux of ethanol in the membrane roughly scales with the

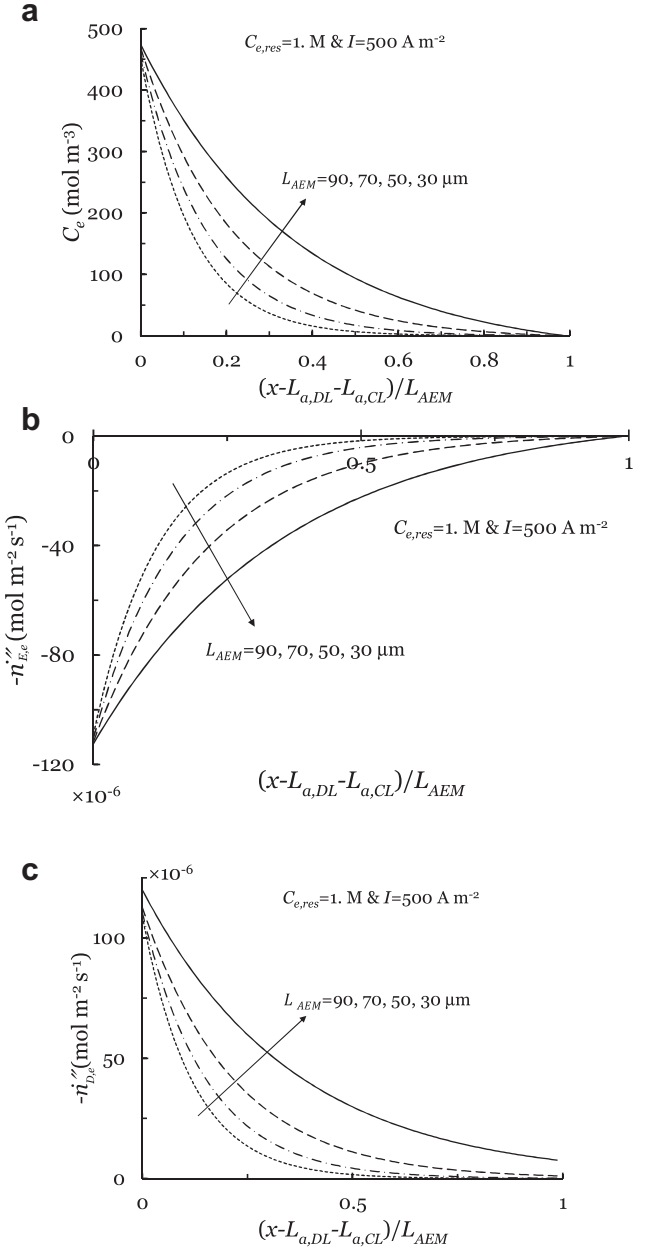


**Fig. 11.** The effect of increase in the membrane thickness on the local distribution of (a) the ethanol concentration, (b) the electroosmotic, and (c) the diffusive flux of ethanol within the membrane, when  $C_{e,res} = 1$  M,  $I = 500$  A m<sup>-2</sup> and  $0.03 \leq L_{AEM} \leq 0.09$  mm.

magnitude of the diffusive transport of that, and the trend for both transport mechanisms is nearly the same.

Poor ion conductivity of the available AEMs is one of the major concerns in the development of AEM-DEFCs. Considering the significant decrease in the ethanol crossover, especially at the higher current densities (**Fig. 7**), decreasing the thickness of the membrane is one of the feasible and effective solutions to the above-noted problem. **Fig. 10(a)** shows the influence of membrane thickness on the ethanol crossover when  $C_{e,res} = 1$  M and  $0.03 \leq L_{AEM} \leq 0.09$  mm. It is illustrated that reducing the thickness of the membrane results in a significant increase in ethanol crossover when  $I \rightarrow 0$ . **Fig. 10(b)** shows the effect of membrane thickness on the cell polarization. At low current densities ( $I \rightarrow 0$ ), the cell performance is deteriorated with decreasing membrane thickness. It is attributed to the higher cathode overpotential due to the

increased ethanol crossover for the thinner membranes. The performance of the cell with thinner membrane, however, increases at the higher current densities for two reasons: (i) lower resistance against  $\text{OH}^-$  transport through the membrane (Eq. (24)), and (ii) negligible ethanol crossover. Therefore, reducing the thickness of the membrane is an effective method to compensate for the poor ion conductivity of AEMs, if the DEFC operates at high current densities.

Fig. 11 shows the local distribution of ethanol concentration, electroosmotic drag and diffusive transport of ethanol in the membrane for  $C_{e,res} = 1 \text{ M}$ ,  $I = 500 \text{ A m}^{-2}$  and  $0.03 \leq L_{AEM} \leq 0.09 \text{ mm}$ . The total ethanol flux,  $\dot{n}_e''$ , made up of the convective (electroosmotic) and diffusive fluxes is:

$$\dot{n}_e'' = C_e u - D_e^{\text{eff}} \frac{dC_e}{dx} \quad (37\text{a})$$

$$u = \frac{I}{n_d F (C_{\text{H}_2\text{O}} + C_e + C_{\text{KOH}})} \quad (37\text{b})$$

Peclet number,  $\text{Pe}$ , is defined as the ratio of the convective to the diffusive flux:

$$\text{Pe} = \frac{u L_{AEM}}{D_{e,\text{mem}} \cdot \epsilon_{\text{mem}}} \quad (38)$$

As evident in Fig. 11(a), ethanol flow through the membrane becomes diffusion dominant, low  $\text{Pe}$ , as the membrane thickness decreases. Fig. 11(b) and (c) illustrate that both electroosmotic and diffusive drags of ethanol in the membrane increase upon a decrease in the membrane thickness. The electroosmotic transport and  $C_e$  distribution in the membrane follow the similar trend, while diffusive transport scales with the local derivative of  $C_e$ .

## 5. Conclusions

A one-dimensional, isothermal, multi-layer membrane model is proposed to study the mass transport in a DEFC using an AEM. The electrochemistry is solved analytically by assuming Tafel expressions for both EOR and ORR. Explicit expressions for the anode and cathode overpotentials are obtained for two limiting cases. From the proposed model, the following conclusions are made:

- Employing a multi-layer membrane model is essential to provide a physical and proper description of mass transport in an AEM-DEFC.
- A substantial difference in ethanol distribution within the membrane exists for the positive and negative electroosmotic drag coefficients.
- A significant decrease in ethanol crossover is observed upon using an AEM compared to using a proton exchange membrane.

- Reducing the membrane thickness is an effective and reliable method to compensate for the low ion conductivity of AEMs, if the DEFC operates at high current densities,  $I \geq 500 \text{ A m}^{-2}$ .

## References

- [1] K. Scott, W.M. Taama, P. Argyropoulos, K. Sundmacher, J. Power Sources 83 (1999) 204–216.
- [2] X. Ren, T.E. Springer, T.A. Zawodzinski, S. Gottesfeld, J. Electrochem. Soc. 147 (2000) 466–474.
- [3] M.M. Verbrugge, J. Electrochem. Soc. 136 (1989) 417–423.
- [4] J. Han, H. Liu, J. Power Sources 164 (2007) 166–173.
- [5] L. Feng, Q. Lv, X. Sun, S. Yao, C. Liu, W. Xing, J. Electroanal. Chem. 664 (2012) 14–19.
- [6] N. Fujiwara, Z. Siroma, S.- Yamazaki, T. Ioroi, H. Senoh, K. Yasuda, J. Power Sources 185 (2008) 621–626.
- [7] H. Hou, G. Sun, R. He, Z. Wu, B. Sun, J. Power Sources 182 (2008) 95–99.
- [8] A.D. Modestov, M.R. Tarasevich, A.Y. Leykin, V.Y. Filimonov, J. Power Sources 188 (2009) 502–506.
- [9] Y.S. Li, T.S. Zhao, Z.X. Liang, J. Power Sources 190 (2009) 223–229.
- [10] Y.S. Li, T.S. Zhao, Z.X. Liang, J. Power Sources 187 (2009) 387–392.
- [11] C. Bianchini, V. Bambagioni, J. Filippi, A. Marchionni, F. Vizza, P. Bert, A. Tampucci, Electrochim. Commun. 11 (2009) 1077–1080.
- [12] V. Bambagioni, C. Bianchini, A. Marchionni, J. Filippi, F. Vizza, J. Teddy, P. Serp, M. Zhiani, J. Power Sources 190 (2009) 241–251.
- [13] S.Y. Shen, T.S. Zhao, J.B. Xu, Y.S. Li, J. Power Sources 195 (2010) 1001–1006.
- [14] Y.S. Li, T.S. Zhao, Int. J. Hydrogen Energy 36 (2011) 7707–7713.
- [15] M. Zhiani, H.A. Gasteiger, M. Piana, S. Catanorchi, Int. J. Hydrogen Energy 36 (2011) 5110–5116.
- [16] P.V. Mazinz, N.A. Kapustina, M.R. Tarasevich, Russ. J. Electrochim. 47 (2011) 275–281.
- [17] S.Y. Shen, T.S. Zhao, J.B. Xu, Energy Environ. Sci. 4 (2011) 1428–1433.
- [18] K. Tadanaga, Y. Furukawa, A. Hayashi, M. Tatsumisago, Adv. Mater. 22 (2010) 4401–4404.
- [19] A.Y. Leykin, O.A. Shkrebko, M.R. Tarasevich, J. Membr. Sci. 328 (2009) 86–89.
- [20] H. Hou, S. Wang, W. Jin, Q. Jiang, L. Sun, L. Jiang, G. Sun, Int. J. Hydrogen Energy 36 (2011) 5104–5109.
- [21] Z.X. Liang, T.S. Zhao, J.B. Xu, L.D. Zhu, Electrochim. Acta 54 (2009) 2203–2208.
- [22] H. Bahrami, A. Faghri, J. Power Sources 196 (2011) 1191–1204.
- [23] A.A. Kulikovsky, Electrochim. Commun. 4 (2002) 318–323.
- [24] A.J. Bard, L.R. Faulkner, Electrochemical Methods, Fundamentals and Applications, second ed. John Wiley & Sons, NJ, USA, 2001.
- [25] F. Weinhold, Classical and Geometrical Theory of Chemical and Phase Thermodynamics, John Wiley & Sons, New Jersey, USA, 2009.
- [26] A.A. Kulikovsky, Electrochim. Commun. 4 (2002) 939–946.
- [27] R. Chen, T.S. Zhao, J. Power Sources 152 (2005) 122–130.
- [28] J.R. Varcoe, R.C.T. Slade, E.L.H. Yee, S.D. Poynton, D.J. Driscoll, J. Power Sources 173 (2007) 194–199.
- [29] C.C. Yang, S.J. Chiu, K.T. Lee, W.C. Chien, C.T. Lin, C.A. Huang, J. Power Sources 184 (2008) 44–51.
- [30] Y.S. Li, T.S. Zhao, W.W. Yang, Int. J. Hydrogen Energy 35 (2010) 5656–5665.
- [31] L. Zhang, Q. Wang, Y.C. Liu, L.Z. Zhang, J. Chem. Phys. 125 (2006) 104502.
- [32] H. Bahrami, A. Faghri, J. Electrochim. Soc. 157 (2010) B1762–B1776.
- [33] R.C.T. Slade, J.R. Varcoe, Solid State Ionics 176 (2005) 585–597.
- [34] R. Lide David; 2005.
- [35] M.J. Moran, H.N. Shapiro, Fundamentals of Engineering Thermodynamics, sixth ed. John Wiley & Sons, NY, 2008.
- [36] C. Xu, T.S. Zhao, W.W. Yang, J. Power Sources 178 (2008) 291–308.
- [37] W.W. Yang, T.S. Zhao, J. Power Sources 174 (2007) 136–147.
- [38] W.W. Yang, T.S. Zhao, J. Power Sources 188 (2009) 433–446.
- [39] W.W. Yang, T.S. Zhao, J. Power Sources 185 (2008) 1131–1140.
- [40] H. Bahrami, A. Faghri, Int. J. Heat Mass Transfer 53 (2010) 2563–2578.
- [41] B. Xiao, H. Bahrami, A. Faghri, J. Power Sources 195 (2010) 2248–2259.
- [42] Z.H. Wang, C.Y. Wang, J. Electrochim. Soc. 150 (2003) A508–A519.
- [43] W.W. Yang, T.S. Zhao, Electrochim. Acta 52 (2007) 6125–6140.
- [44] J.P. Meyers, J. Newman, J. Electrochim. Soc. 149 (2002) A729–A735.